Electrical Power and Energy Systems 120 (2020) 105959

Contents lists available at ScienceDirect

Electrical Power and Energy Systems

journal homepage: www.elsevier.com/locate/ijepes

Reactive power management for microgrid frequency control

Saeed Aminzadeh[a], Mehrdad Tarafdar Hagh[a,b,*], Heresh Seyedi[a]

[a] Faculty of Electrical and Computer Engineering, University of Tabriz, 29 Bahman Blvd, Tabriz, Iran
[b] Engineering Faculty, Near East University, 99138 Nicosia, North Cyprus, Mersin 10, Turkey

ARTICLE INFO

Keywords:
Frequency control
Frequency-reactive power channel
Frequency-reactive power factor
Islanded MG
Reactive power management
Virtual spinning reserve

ABSTRACT

In this paper, a frequency-reactive power channel (FRCh) is proposed for improving the performance of conventional frequency control system in an islanded MicroGrid (MG). Using this channel, it will be possible to take advantage of reactive power management for frequency control, in addition to the conventional methods of using active power. In order to create the mentioned channel, a frequency-reactive power controller (FRC) is proposed for controlling the inverter-interfaced energy storage devices. The proposed controller reduces the MG frequency decline during contingencies.

Moreover, it reduces the power of battery employed for the frequency control, while maintaining the customer voltage within permissible limits. Furthermore, this paper defines a new frequency-reactive power factor (FRF) capable of determining the best place for installation of FRC. This factor indicates the dependence of microgrid frequency on reactive power variations in each bus and identifies the buses which are more effective on the MG frequency. To demonstrate the effectiveness of proposed method and the accuracy of new factor, it is implemented on a test network in MATLAB/Simulink environment.

1. Introduction

Microgrid refers to a low voltage distribution network that includes small scale generation sources, energy storage devices, controllable and uncontrollable loads, local controllers, central controller as well as a telecommunication system. MGs are normally connected to the main grid, while in emergency situations they may operate in islanded mode. Hence, MGs are considered as active flexible cells in an electric power system [1]. In the islanded mode of operation, the management of balance between active power generation and consumption for frequency control and similary, the management of balance between reactive power generation and consumption for voltage control are essential. Frequency and voltage control in islanded grids can be accomplished by means of various control methods, either with or without communication [2].

If communication links are not available, frequency and voltage droop control methods will be appropriate choices for the coordinated control of the associated inverters. The droop control method, which has attracted the attention of many researchers, is applicable when the inductive component of line impedances is dominant over the resistive component [1,3–12]. This condition is satisfied only in high voltage systems where the R/X ratio is small. However, in a low voltage MG, the required condition for the application of conventional droop control is no longer retained, due to the high R/X ratio of line impedance. This may result in the deterioration of the dynamic response of the controller, due to the coupling between the equations of active and reactive powers, which might jeopardize system stability [2,3]. In order to deal with this problem in low voltage MGs, a number of improved droop control methods have been proposed to decouple the equations of active and reactive powers of the inverter.

The first method is known as the virtual power based decoupling method. The virtual power based control scheme is widely used for dealing with the above problem in the low voltage MG, which could decouple the power flow equations by appropriate rotation of the power vectors. The virtual active and reactive powers are, respectively, related to the frequency and voltage amplitude. [2,3,13–17]. Transformation from the virtual power to the actual power depends on the impedance angle of the transmission line connected to the inverter which is not identical for all inverters. Thus, the actual power may not be shared equally. Therefore, the main issue of the virtual power based method is that the actual power sharing performance heavily relies on the consistence of line impedance angles of the inverters [3]. Decoupled power control is simply based on the line impedance. However, the load characteristics may also generate power coupling and alter the equivalent system impedance characteristic [15]. In addition, those droop relationships are enforced only during the system transient. In

* Corresponding author.
E-mail address: tarafdar@tabrizu.ac.ir (M. Tarafdar Hagh).

https://doi.org/10.1016/j.ijepes.2020.105959
Received 7 March 2019; Received in revised form 21 December 2019; Accepted 21 February 2020

Nomenclature

FRF_i	frequency reactive power factor of the i-th bus in (Hz/MVar).
f_{MG}	MG frequency in (Hz).
P_{bat}	total active load on the battery in (kW).
$P_{loadtotal}$	total active load of the MG in (kW).
P_{loadj}	active load connected to the j-th bus in (kW).
$\|V_j\|$	voltage magnitude of the j-th bus in (p. u.).
$\|V_k\|$	voltage magnitude of the k-th bus in (p. u.).
Q_{bat}	reactive power on the battery in (kVar).
Q_i	reactive load connected to the i-th bus in (kVar).
ΔQ_i	reactive power changes of the i-th bus in (kVar).
Δf_{MG}	MG frequency changes in (Hz).
f_{0MG}	MG frequency when $P_{bat} = 0$ in (Hz).
$\|V_{0k}\|$	battery voltage magnitude when $Q_{bat} = 0$ in (p. u.).
K_q	droop slope of active power in (Hz/kW).
K_q	droop slope of reactive power in (p. u. /kVar).
Q_{0j}	reactive power consumption of the j-th bus at the voltage V_{0j} in (kVar).
P_{0j}	active power consumption of the j-th bus at the voltage V_{0j} in (kW).
a	dependency coefficient of the active power of loads on voltage magnitude.
b	dependency coefficient of the reactive power of loads on voltage magnitude.
K_{pf}	coefficient of dependence of active power consumption on frequency variations
P	output active power of the inverter in (kW).
Q	output reactive power of the inverter in (kVar).
ω_0	angular frequency when the inverter output power is zero in (rad/s).
V_0	terminal voltage magnitude when the inverter output power is zero in (p. u.).
V	reference voltage magnitude in (p. u.).
ω	reference angular frequency in (rad/s).
K_{FRC}	coefficient indicating the degree of FRC participation in the frequency control.
V_{CBEMA}	voltage magnitude corresponding to the CBEMA curve in (p. u.).
$\Delta\omega_{limit}$	acceptable angular frequency variation in (rad/s).

steady state, only the standard active power versus frequency and reactive power versus voltage droop relationships define the power sharing [17].

The Second method is known as the virtual impedance based decoupling method. In this method, a large virtual inductance is exploited at the output terminals of the inverter to modify the equivalent output impedance to make it predominantly inductive. To avoid the coupling between active and reactive powers, virtual impedance methods have been proposed to make the output impedance of the inverter highly inductive [18–22]. However, it is a challenging issue to design the virtual impedance value with the least possible complexity which can effectively decouple the power flow equations and, at the same time, maintain satisfactory system dynamics and stability [3]. The main problem in using virtual impedance method is associated with the aggravation of reactive power sharing, due to the increased voltage drops [18].

The Third method is referred to as the virtual frequency and voltage based decoupling method. This method is similar to the virtual power based decoupling method [23]. The frequency and voltage amplitude are transformed into a virtual frame to build a new relationship with, respectively, the active and the reactive power. However, the paper does not provide a mathematical derivation to prove that the power flows are decoupled in the virtual frequency and voltage frame [3].

Given the drawbacks of the above-mentioned improved droop control methods, this paper seeks to provide a different and simple idea for improving the performance of conventional droop control method to control the frequency of a MG. The conventional frequency control system is not sufficient to control the frequency of a MG for the following reasons. Hence, a complementary control scheme is required to improve the performance of conventional frequency control.

- In a MG, the overall network inertia is considerably low, which is due to the power electronic-interfaced power supply resources. Hence, the frequency drop will be faster,
- The energy of MGs is widely supplied by the renewable energy sources, which usually operate at the maximum power point,
- In a MG, resources such as fuel cells and micro-turbines that allow frequency control through active power introduce low response rates,
- In a MG, resources such as batteries that allow fast control over active power have a high cost of construction and maintenance.

In this paper, the idea of using reactive power control for improving the performance of conventional frequency control system during a transient and emergency period is presented. As such, a frequency-reactive power channel is created, considering three fundamental principles listed below:

- Dependence of the MG frequency on the active power consumed by the loads,
- Dependence of the active power consumed by the loads on the MG bus voltages,
- Dependence of the MG bus voltages on the reactive power generated in the MG.

To create the mentioned channel, a novel frequency-reactive power controller (FRC) is proposed and added to the conventional frequency control system. This addition may entail the following advantages:

- The MG frequency would undergo a smaller drop after disconnection of the MG from the upstream grid and would return to its nominal value in shorter time,
- The power of battery used to control the frequency is reduced,
- The consumer voltage would remain within allowable limits and would comply with established standards,
- There would be no need for load shedding at the instant of disconnection from the upstream grid.

Indeed, FRC is principally an emergency control scheme. In other words, at the critical moments (such as the moment of disconnection from the upstream network, where fast frequency control is very important to prevent the frequency instability) with the aid of reactive power management, FRC changes the MG voltage magnitude. This deliberate change of the MG voltage magnitude helps to control the MG frequency faster and more effectively. in other words, during emergency conditions after islanding, with the deliberate decrease/increase in the voltage magnitude, active power consumption of the Controllable loads decreases/increases. This will balance the active power generation-consumption. Meanwhile, the voltage magnitude variations should always be within the allowed range and according to the relevant standards (such as the well- known CBEMA and ITIC curves). In the steady state condition, the voltage magnitude is also returned to the nominal value as the frequency returns to its nominal value. It should be noted that since the majority of renewable energy sources in the

microgrid are inverter-interfaced, reactive power control for the purpose of frequency control will not be difficult.

The proposed control scheme is applied to the critical buses. The buses in which variation of reactive power produces significant change in the MG frequency are designated as critical buses. A frequency-reactive power factor (FRF) is introduced for this purpose and the required mathematical formulations are presented. For each bus, this factor indicates the dependence of the MG frequency on the variation of reactive power injected to that bus. FRF and FRC are the newly proposed concepts that have not been mentioned in any previous research works. These concepts are in accordance with the three fundamental principles mentioned above. Major contributions of this paper may be summarized as the following:

- The idea of manipulating the active power consumption of loads through voltage control has been proposed to improve the performance of conventional frequency control system during emergency situations.
- The well-known CBEMA curve allows short duration voltage drops in the system. This permission has been exploited in this work to deliberately decrease the voltage magnitudes of selected buses in the system, for a very short period of time. This way, frequency stability is improved in emergency situations.
- The frequency-reactive power controller (FRC) has been proposed to be added to the conventional frequency control system to improve its performance.
- The frequency-reactive power factor (FRF) has been proposed. This factor can be used to determine the sensitivity of MG frequency to the reactive power change in each bus.

The rest of the paper is organized as follows: in the second section, a new factor is introduced and the method of its extraction is explained. In the third section, the proposed frequency control method is explained. In Section 4, results of simulation studies on a sample independent grid are presented, to demonstrate the accuracy of new factor and the effectiveness of proposed method. Finally, in Section 5, major conclusions of the paper are presented.

2. The proposed frequency-reactive power factor

A factor, FRF, can be defined according to (1) for each bus of an islanded MG.

$$FRF_i = \frac{\partial f_{MG}}{\partial Q_i} = \frac{\partial f_{MG}}{\partial P_{bat}} \times \left(\frac{\partial P_{bat}}{\partial P_{loadtotal}}\right)_i \times \frac{\partial P_{loadtotal}}{\partial Q_i} = \frac{\partial f_{MG}}{\partial P_{bat}} \times \left(\frac{\partial P_{bat}}{\partial P_{loadtotal}}\right)_i \times \sum_{j=1}^{n} \left[\frac{\partial P_{loadj}}{\partial |V_j|} \times \frac{\partial |V_j|}{\partial |V_k|} \times \frac{\partial |V_k|}{\partial Q_{bat}} \times \frac{\partial Q_{bat}}{\partial Q_i}\right] \quad (1)$$

FRF indicates the sensitivity of MG frequency to the variations of reactive power at each bus. In this case, it is assumed that there is only one battery and that battery is connected to the k-th bus. FRF indicates that if the reactive power in the i-th bus changes by ΔQ_i, the MG frequency changes by $\Delta f_{MG} = FRF_i \times \Delta Q_i$. In fact, this factor shows the degree of dependence of the MG frequency on reactive power changes of i-th bus. The coefficients $\left(\frac{\partial f_{MG}}{\partial P_{bat}}\right)$, $\left(\frac{\partial P_{bat}}{\partial P_{loadtotal}}\right)_i$, $\left(\frac{\partial P_{loadj}}{\partial |V_j|}\right)$, $\left(\frac{\partial |V_j|}{\partial |V_k|}\right)$, $\left(\frac{\partial |V_k|}{\partial Q_{bat}}\right)$ and $\left(\frac{\partial Q_{bat}}{\partial Q_i}\right)$ should be calculated and substituted in Eq. (1) in order to obtain FRF for the i-th bus.

Voltage source inverters (VSI) are frequently used in order to connect a storage device to the MG. the VSI acts as a voltage source, with the magnitude and frequency of the output voltage controlled through droops, as described in the following equations [1]:

$$f_{MG} = f_{0MG} - (K_p \times P_{bat}) \quad (2)$$

$$|V_k| = |V_{0k}| - (K_q \times Q_{bat}) \quad (3)$$

Using (2) and (3), we have:

$$\frac{\partial f_{MG}}{\partial P_{bat}} = -K_P \quad (4)$$

$$\frac{\partial |V_k|}{\partial Q_{bat}} = -K_q \quad (5)$$

To model the dependency of active and reactive powers of MG loads on voltage magnitude, the exponential load model is used as follows [24]:

$$P_{loadj} = P_{0j} \times \left(\frac{|V_j|}{|V_{0j}|}\right)^a \quad (6)$$

$$Q_{loadj} = Q_{0j} \times \left(\frac{|V_j|}{|V_{0j}|}\right)^b \quad (7)$$

Differentiating (6) in terms of $|V_j|$, yields:

$$\frac{\partial P_{loadj}}{\partial |V_j|} = a \times \left(\frac{P_{0j}}{|V_{0j}|}\right) \times \left(\frac{|V_j|}{|V_{0j}|}\right)^{a-1} \quad (8)$$

When a bus voltage changes, voltages of other buses correspondingly change. In this paper, it has been assumed that when the reactive power injected into one bus changes, the currents injected into the other bus are constant. As a result, changes in the voltage magnitude of the j-th bus, due to changes in the k-th bus voltage magnitude, are calculated by the following equation [25]:

$$\Delta |V_j| = \Delta |V_k| \times \left(\frac{|Z_{jk}|}{|Z_{kk}|}\right) \quad (9)$$

To obtain $(\frac{\partial Q_{bat}}{\partial Q_i})$, (3) is used as the following:

$$|V_k| - |V_{0k}| = \Delta |V_k| = -K_q \times Q_{Bat} \quad (10)$$

From (9):

$$\Delta |V_i| = |V_i| - |V_{0i}| = \left(\frac{|Z_{ik}|}{|Z_{kk}|}\right) \times \Delta |V_k| \quad (11)$$

By replacing (10) in (11):

$$|V_i| = |V_{0i}| + \left(\frac{|Z_{ik}|}{|Z_{kk}|} \times -K_q \times Q_{Bat}\right) \quad (12)$$

From (7):

$$Q_i = Q_{0i} \times (\frac{|V_i|}{|V_{0i}|})^b \quad (13)$$

By replacing (12) in (13):

$$Q_i = Q_{0i} \times [\frac{|V_{0i}| + \left(\frac{|Z_{ik}|}{|Z_{kk}|} \times -K_q \times Q_{Bat}\right)}{|V_{0i}|}]^b \quad (14)$$

Differentiating (14) with respect to Q_{Bat},yields:

$$\frac{\partial Q_i}{\partial Q_{bat}} = \left(\frac{b \times Q_{0i}}{|V_{0i}|^b}\right) \times \left(\frac{-K_q \times |Z_{ik}|}{|Z_{kk}|}\right) \times \left[|V_{0i}| + \left(\frac{|Z_{ik}|}{|Z_{kk}|} \times -K_q \times Q_{Bat}\right)\right]^{b-1} \quad (15)$$

By reversing (15):

$$\frac{\partial Q_{bat}}{\partial Q_i} = \frac{1}{\left(\frac{b \times Q_{0i}}{|V_{0i}|^b}\right) \times \left(\frac{-K_q \times |Z_{ik}|}{|Z_{kk}|}\right) \times \left[|V_{0i}| + \left(\frac{|Z_{ik}|}{|Z_{kk}|} \times -K_q \times Q_{Bat}\right)\right]^{b-1}} \quad (16)$$

To calculate $\left(\frac{\partial P_{bat}}{\partial P_{loadtotal}}\right)$, from (2) we have:

$$f_{MG} - f_{0MG} = \Delta f = (-K_p \times P_{bat}) \quad (17)$$

From (12):

$$|V_j| = |V_{0j}| + \left(\frac{|Z_{jk}|}{|Z_{kk}|} \times -K_q \times Q_{Bat}\right) \tag{18}$$

Active power consumption of loads is dependent not only on the voltage variations but also on the frequency variations. In (6), for simplicity, frequency dependence has been neglected. Considering this dependence, the complete equation will be as follows:

$$P_{loadj} = (P_{0j}) \times \left(\frac{|V_j|}{|V_{0j}|}\right)^a \times (1 + (K_{pf} \times \Delta f)) \tag{19}$$

The total active demand of loads is obtained through the following equation:

$$P_{loadtotal} = \sum_{j=1}^{n} (P_{loadj}) \tag{20}$$

By replacing (17)–(19) in (20):

$$P_{load\ \ total} = \sum_{j=1}^{n} \left[(P_{0j}) \times \left(\frac{|V_{0j}| + \left(\frac{|Z_{jk}|}{|Z_{kk}|} \times -K_q \times Q_{Bat}\right)}{|V_{0j}|} \right)^a \times (1 - (K_{pf} \times K_p \times P_{bat})) \right] \tag{21}$$

Differentiating (21) with respect to P_{Bat}, yields:

$$\frac{\partial P_{load\ \ total}}{\partial P_{bat}} = (-K_{pf} \times K_p) \times \sum_{j=1}^{n} [P_{0j} \times \left\{ \frac{|V_{0j}| + \left(\frac{|Z_{jk}|}{|Z_{kk}|} \times -K_q \times Q_{Bat}\right)}{|V_{0j}|} \right\}]^a \tag{22}$$

By reversing (22), we have:

$$\frac{\partial P_{bat}}{\partial P_{load\ \ total}} = \frac{1}{[(-K_{pf} \times K_p) \sum_{j=1}^{n} [P_{0j} \times \left\{ \frac{|V_{0j}| + \left(\frac{|Z_{jk}|}{|Z_{kk}|} \times -K_q \times Q_{Bat}\right)}{|V_{0j}|} \right\}]^a} \tag{23}$$

An equation for calculating FRF of each bus can be obtained by replacing equations (4), (5), (8), (9), (16) and (23) in (1). It should be noted that the calculation of the proposed FRF is dependent on the initial location of the battery and the type of frequency or voltage control system. But this dependency is not a problem. Because first, the initial location of the battery can be easily achieved using the steady-state power flow analysis and second, the type of control system is chosen according to the purpose. The purpose of this paper is to improve the performance of the conventional droop control, which is why this type of control system has been used in the calculation of the FRF. Of course, the proposed FRF is flexible and can be applied with slight modifications for other types of control systems. Also, the proposed FRF has less computational complexity than similar relationships.

3. The proposed frequency control method

When the MG is connected to the upstream network, inverters of the renewable energy sources operate in the PQ control mode, and the voltage magnitude and frequency references are determined, assuming the upstream network as an infinite bus. However, as soon as the MG disconnects from the upstream network, the VSI inverter provides new references for voltage magnitude and frequency. The VSI inverter typically interfaces between storage devices (such as a flywheel and battery) and the AC network. Using the energy stored in these devices, the VSI can have a performance similar to a synchronous generator. Therefore, it can control the voltage magnitude and frequency in the isolated MG. In this case, the references of frequency and voltage magnitudes are calculated through the following equations:

$$\omega = \omega_0 - (K_p \times P) \tag{24}$$

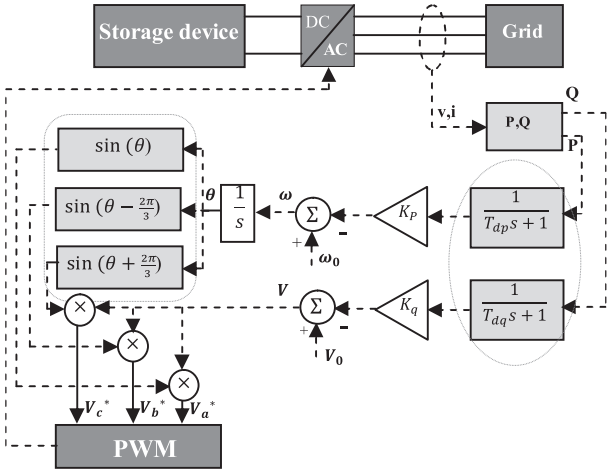

Fig. 1. Conventional VSI control model.

$$V = V_0 - (K_q \times Q) \tag{25}$$

The conventional VSI control model functions are implemented based on (24) and (25) for MG control in the islanded mode of operation, as shown in Fig. 1.

A frequency reactive power controller (FRC) is proposed in this paper to take advantage of the reactive power potential in order to control the frequency of a MG. FRC creates a frequency-reactive power channel. By adding this control system to the conventional VSI control model, in case of any disconnection from the upstream network, the slope of frequency reduction decreases and frequency drop decreases as well. The proposed VSI control model is shown in Fig. 2. In this model, if the V_{FRC} signal is added to (25), the following equation will be obtained:

$$V = V_0 - (K_q \times Q) - V_{FRC} \tag{26}$$

This added signal leads to a reduction in V in accordance with ω deviation with respect to the ω_0 at the moment of disconnection from the upstream network. This signal is calculated using the following equation:

$$V_{FRC} = K_{FRC} \times (\omega - \omega_0) \times [-V_{CBEMA} + V_0 - (K_q \times Q)] \tag{27}$$

$$K_{FRC} = \frac{1}{\Delta\omega_{limit}} \tag{28}$$

As soon as ω value deviates from ω_0, FRC is activated and generates the V_{FRC} signal to change V in order to enhance the frequency control.

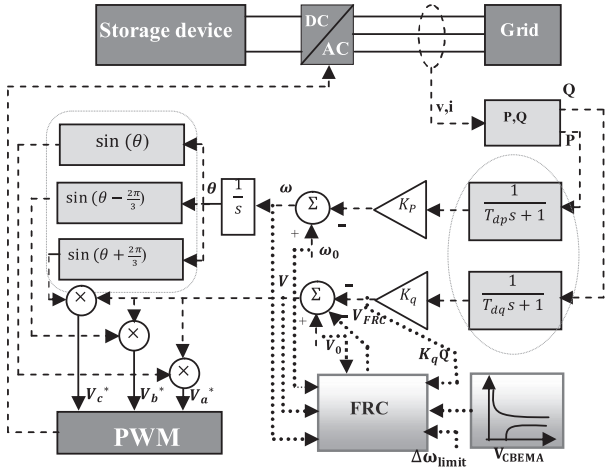

Fig. 2. Proposed VSI control model.

The value of this signal is selected so that V remains in the allowed limit and the voltage is in accordance with the relevant standards. The CBEMA curve, is shown in Fig. 3, can be used to assess the voltage quality in the case of a voltage drop / voltage rise. The CBEMA Curve shows how long the voltage magnitude is allowed to deviate from its rated value [26]. In this paper, the time period V is allowed to deviate from V_0 in order to enhance the frequency control, is always in full compliance with this curve. V_{CBEMA} is placed in (27) for this purpose. One of the main benefits of proposed FRC is its simple implementation and very little cost. As a result, the FRC can be installed in a system on more than one bus with reactive power generation sources.

By decreasing the voltage magnitude and consequently reduction in the active power consumption, the balance between active power generation and consumption in the MG is restored fast as possible and the frequency drop will stop quickly. By stopping the frequency drop, the power should be transferred from the energy storage device to the controllable generation sources such as fuel cells and microturbines. This can be accomplished by a secondary frequency control system, as shown in Fig. 4. In this system, the amount of active power that must be generated by each microsource (MS) to return the frequency to the nominal value is controlled and applied by the microsource controller (MC), installed at a controllable power supply. Hence, the load is removed from the storage system and the frequency returns to the nominal value through this power generation.

4. Simulation results

4.1. Simulation results for FRF

In order to demonstrate the effectiveness and accuracy of FRF, simulations are carried out for a sample 13-bus microgrid, as shown in Fig. 5. In normal conditions, the microgrid is connected to the upstream network and the power output of battery is zero. The MG is disconnected from the upstream network after fault occurrence in the main grid, and the imbalance between power generation and consumption is compensated by a battery in Bus 3. This microgrid is part of a 400 V distribution network and contains a 50 kW solid oxide fuel cell (SOFC) and a 10 kW photovoltaic (PV) array. Total active and reactive loads of the MG equal to 60 kW and 25 kVar, respectively. Due to the short line lengths in the microgrids, the capacitances of the lines are ignored. The information related to the lines and loads are, respectively, reported in Tables 1 and 2. In order to conduct the desired tests, the sample microgrid is simulated in the MATLAB/Simulink environment considering the nominal frequency of the system equal to 50 Hz. Moreover, the other parameters are assumed as follows: $K_p = 1.2566 \times 10^{-4}$ Rad/(s. W), $K_q = 3 \times 10^{-6}$ p. u/Var, a = 2, b = 2, and $K_{pf} = 1.8$.

FRF is obtained for each bus using Eq. (34), and the values are shown in descending order in Table 3. It may be concluded from the values shown in this table that injection of reactive load to Bus 3 has the largest effect, while injection to Bus 4 has the smallest effect on the microgrid frequency. Therefore, in order to manage the reactive power for frequency control, one may assign the most priority to Bus 3 and the least priority to Bus 4.

To demonstrate the accuracy of the proposed FRF, the reactive power injected to each bus is changed by 50 kVar, and the microgrid frequency is measured each time. The measured value is compared with the proposed value using FRF, and the percentage of error between the two values is calculated. The results are reported in Table 4. Considering the error percentages of all buses, it may be concluded that, using FRF, one can predict with high accuracy the sensitivity of frequency to the changes in the reactive power injected to each bus and use it to optimally and effectively manage the reactive power in order to control the frequency of a microgrid.

4.2. Simulation results for the frequency-reactive power controller

To demonstrate the superiority of the proposed frequency-reactive power controller compared to the conventional controller, the sample microgrid shown in Fig. 5 is employed. The battery, the source of reactive power generation used in the proposed frequency-reactive power controller, is installed in “Bus 3”, which possesses the highest FRF according to Table 3. In this paper, battery due to its power electronics interface, in addition to the active power source is also considered as a source of reactive power and, that is why the battery has sited based upon the FRF. Generally speaking, The optimal siting of the battery is typically carried out based upon the normal (with the system frequency maintained at the nominal value) steady-state power flow analysis by looking into the bus voltage profile, network loss, space convenience and so on. It is assumed that the microgrid is initially connected to the upstream grid, and the steady-state voltage and frequency of the microgrid are equal to those of the upstream grid. The steady-state distribution of the active and reactive powers generated and consumed by the various components of the microgrid are shown in Table 5. The microgrid is suddenly disconnected from the upstream grid at time $t = 10(s)$. In this situation, the balance between generation and consumption of active power in the microgrid is lost, and the frequency starts to decrease since the power cannot be transferred from the upstream grid into the microgrid. At this instant, the battery, which is a source of rapid power generation, acts as a primary frequency controller, preventing a frequency drop and maintaining it at a value smaller than the initial nominal value. Then, the secondary frequency control system is engaged, transferring the load from the battery to the SOFC (as the source of slow controllable power generation) and returning the frequency to its nominal value. Here, three different scenarios are conceived:

Scenario 1. In the mentioned frequency control process, the voltage makes no contribution and always remains at its nominal value.
Scenario 2. To control the frequency after disconnection from the upstream grid, the conventional frequency control system shown in Fig. 1 is used.
Scenario 3. To control the frequency after disconnection from the upstream grid, the proposed frequency control system shown in Fig. 2 is used.

Fig. 6 shows the microgrid frequency in various scenarios. It is clearly understood from this figure that “Scenario 3” demonstrates a significantly better performance in frequency control after disconnection from the upstream grid. The use of proposed controller in this scenario has resulted in the microgrid frequency undergoing a smaller drop after disconnection compared to the other scenarios. Thus, the permissible limits of frequency are not exceeded when the proposed method is applied. This prevents the outages of power generation sources due to frequency reduction and leaves a longer time for the

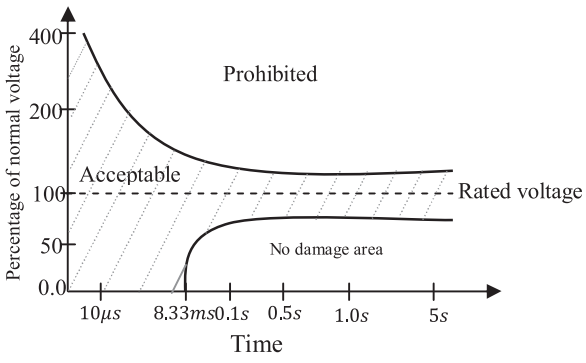

Fig. 3. CBEMA curve.

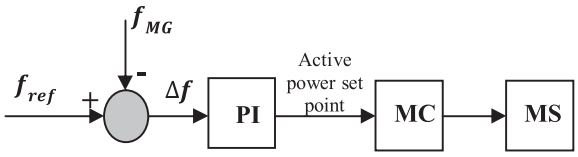

Fig. 4. Secondary frequency control system.

secondary frequency controller to be engaged and to return the frequency to its nominal value. It is also observed that "Scenario 1" in which the voltage is considered as a constant value, has the worst performance, demonstrating the positive effect of voltage participation in the frequency control. Further, the frequency fluctuations after the contingency occurrence at the upstream network are smaller in "Scenario 3", and the frequency returns to its nominal value with a milder slope. Fig. 7 shows the active power output of the battery in various scenarios. It is clearly observed in this figure, that the battery has produced a smaller active power after disconnection in "Scenario 3". In fact, by receiving assistance from the reactive power and reducing load consumption using voltage reduction in this scenario, the required active power has reduced, and a virtual storage capacity of active power has been created in the system. Thus, using the proposed method, lower capacity batteries can be utilized in the microgrid. Due to the costs associated with the purchase, maintenance, and storage of the batteries and the environmental issues related to their disposal after their lifetime, this can lead to a considerable reduction in the operational costs of the microgrid. In all the mentioned scenarios, after stabilizing the frequency at a value smaller than the system nominal value, the secondary frequency controller is engaged. This controller, simultaneously, returns the frequency to its nominal value and transfers the power generation from the batteries to controllable power generation sources such as the SOFC in a continuous manner, reducing the active power generated by the battery to zero. Fig. 8 shows the reactive power generated by the battery in various scenarios. As shown in the figure, the battery continuously produces a constant reactive power equal to the value provided by the grid prior to the disconnection (25 kVar) in the first and second scenarios. However, due to the management of the reactive power output of the battery in the third scenario especially immediately after the disconnection, this potential is used to enhance the frequency control. Nevertheless, the required 25 (kVar) reactive power is provided by the battery inverter in this scenario. The steady-state performance of the battery reactive power is similar in the three scenarios, and the reactive load, unlike the active one, is supplied by

Table 1
Line length (L_{nm}) and impedance (Z_{nm}).

n	m	L_{nm}(M)	Z_{nm}(Ω)
4	1	30	0.024 + j0.0023
4	9	30	0.024 + j0.0023
4	5	100	0.028 + j0.0083
5	10	30	0.024 + j0.0023
5	6	100	0.028 + j0.0083
6	2	30	0.024 + j0.0023
6	11	30	0.024 + j0.0023
6	7	100	0.028 + j0.0083
7	12	30	0.024 + j0.0023
7	8	100	0.028 + j0.0083
8	3	30	0.024 + j0.0023
8	13	30	0.024 + j0.0023

Table 2
The details of active (P_{load}) and reactive (Q_{load}) consumption of the ith bus.

i	P_{load} (kW)	Q_{load} (kVar)
9	10	4
10	15	6
11	15	6
12	10	5
13	10	4

Table 3
FRFs for the buses of the sample microgrid.

Bus number	FRF (Hz/MVar)
3	7.7277
2	7.6079
10	6.2026
13	5.9639
6	5.8423
5	5.5913
1	5.4831
7	5.4578
9	5.3722
8	5.2890
11	5.0859
12	4.6807
4	4.4590

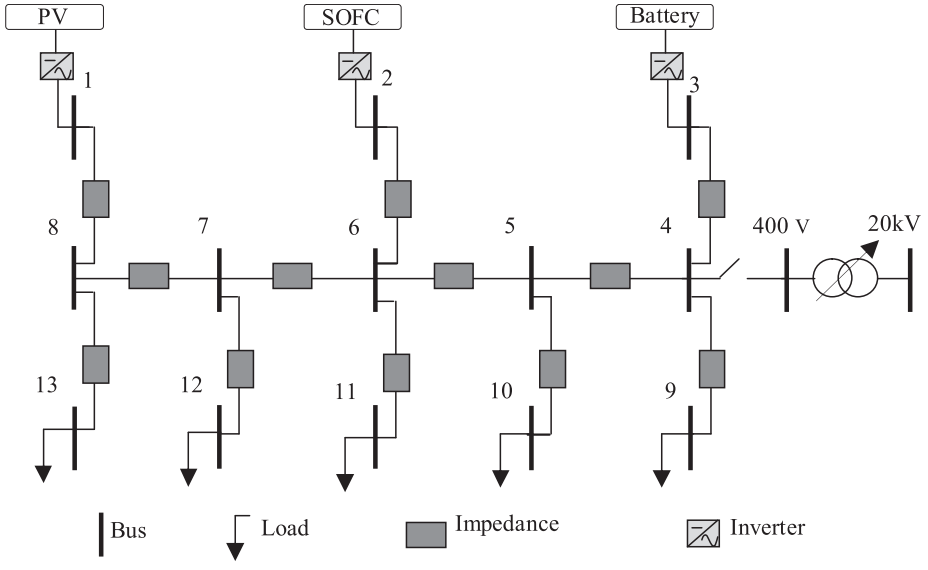

Fig. 5. Sample low-voltage microgrid with 13 buses.

Table 4
Values of FRF, expected frequency, actual frequency, and percent error for the buses of the sample microgrid.

Bus number	FRF (Hz/MVar)	ΔQ_i (*kVar*)	Expected frequency (Hz)	Actual frequency (Hz)	Error (%)
3	7.7277	50	50.3863	50.2732	0.224
2	7.6079	50	50.3803	50.2724	0.214
10	6.2026	50	50.3101	50.2722	0.075
13	5.9639	50	50.2981	50.2668	0.062
6	5.8423	50	50.2921	50.2669	0.050
5	5.5913	50	50.2795	50.2718	0.015
1	5.4831	50	50.2741	50.2719	0.004
7	5.4578	50	50.2728	50.2716	0.002
9	5.3722	50	50.2686	50.2698	0.002
8	5.2890	50	50.2644	50.2677	0.006
11	5.0859	50	50.2542	50.2713	0.034
12	4.6807	50	50.2340	50.2712	0.073
4	4.4590	50	50.2229	50.2781	0.109

Table 5
Distribution of active and reactive powers of different components within the sample microgrid.

Components	Active power generated (kW)	Reactive power generated (kVar)	Active power consumed (kW)	Reactive power consumed (kVar)
Battery	0	0	0	0
SOFC	25	0	0	0
PV	10	0	0	0
Total load	0	0	60	25
Upstream grid	25	25	0	0
Total	60	25	60	25

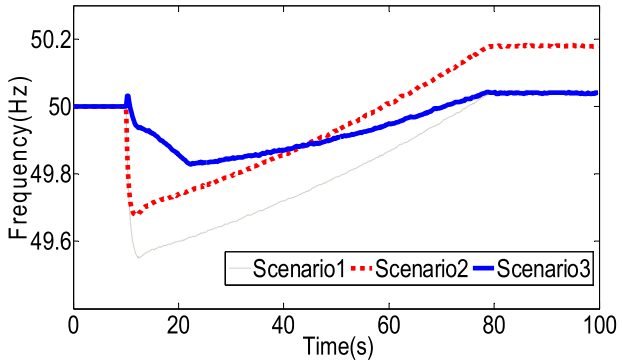

Fig. 6. Microgrid frequency in various scenarios.

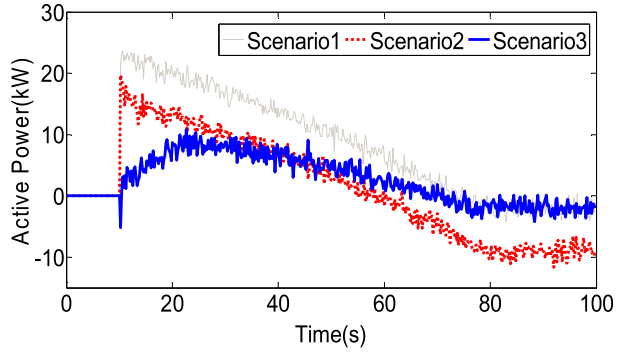

Fig. 7. Battery active power in various scenarios.

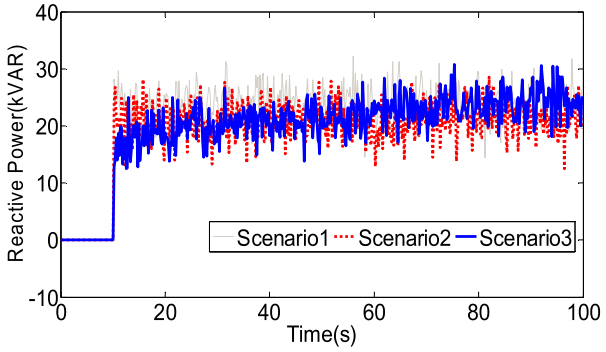

Fig. 8. Battery reactive power in various scenarios.

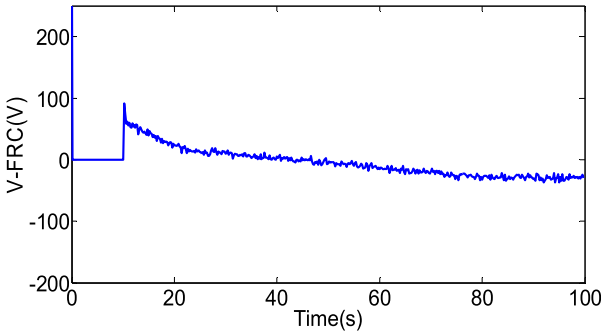

Fig. 9. V_{FRC} signal used in the third scenario.

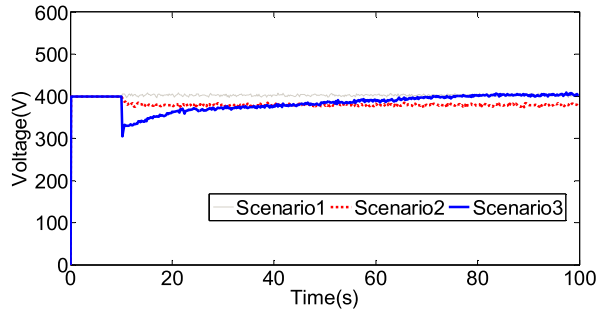

Fig. 10. Magnitude of battery bus voltage in various scenarios.

the battery in all scenarios. In the proposed frequency control system used in the third scenario, an auxiliary signal denoted V_{FRC} is used, as shown in Fig. 9. Fig. 10 shows the magnitude of the battery bus voltage in the three scenarios. This voltage is in fact the reference voltage created by the battery for the microgrid after disconnection from the upstream grid.

Figs. 11–17 illustrate the voltages of SOFC bus, PV bus and some other load buses in different scenarios. Due to the short distances between the buses of this microgrid, the voltage magnitudes of different buses are close to each other and almost similar. It is observed in these figures that voltage magnitudes are constant and equal to 400 V before and after the disconnection in “Scenario 1”. In “Scenario 2”, the magnitude of voltage is equal to the voltage of the upstream grid, 400 V, before the disconnection. However, it reduces to 380 V in proportion with the droop slope of the reactive power considered for the control system after the disconnection and remains constant at this value. Comparing the voltage to the CBEMA curve in “Scenario 3”, it is confirmed that the voltage of this bus complies with the standard and does not exceed permissible limits. Severe drop in voltage for a specific short time interval is allowed according to this standard. For this reason, the severe voltage drop observed in this scenario after the disconnection is acceptable. After a short time interval and as soon as the frequency

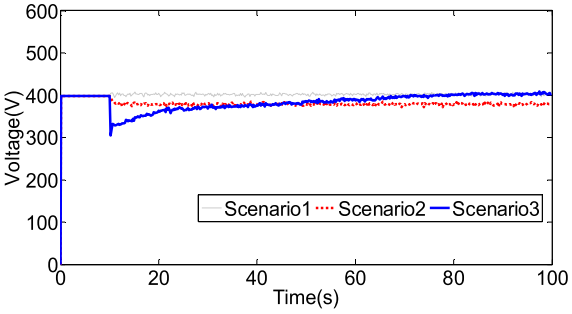

Fig. 11. Magnitude of SOFC bus voltage in various scenarios.

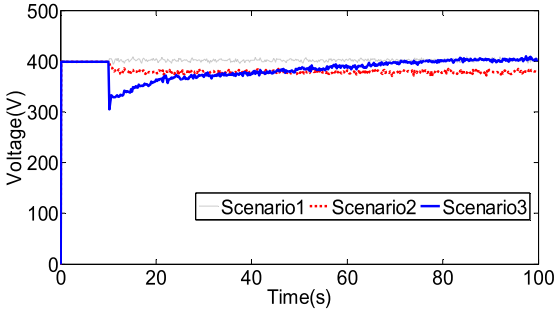

Fig. 12. Magnitude of PV bus voltage in various scenarios.

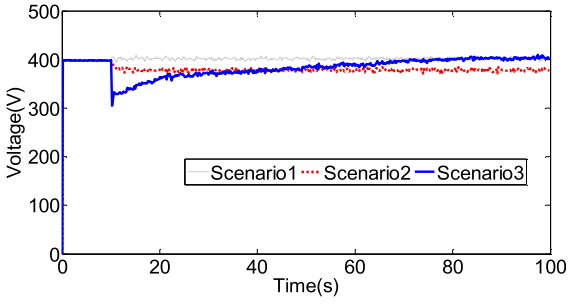

Fig. 13. Magnitude of Bus 13 voltage in various scenarios.

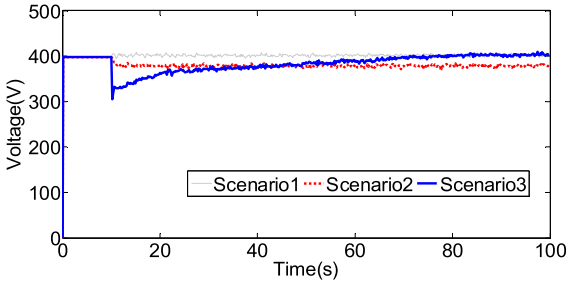

Fig. 14. Magnitude of Bus 12 voltage in various scenarios.

stabilizes, the voltage moves toward its nominal value as the frequency does the same. Moreover, when the frequency reaches its nominal value, the voltage does the same.

Fig. 18 displays the active power output of the SOFC in various scenarios. The SOFC behaves almost similarly in all scenarios. Its active power output is 25 kW prior to the disconnection and reaches 50 kW in the islanded mode of operation of microgrid. Fig. 19 shows the reactive power output of the SOFC in these scenarios. This output is almost the same and equals to zero in all scenarios before and after the disconnection. This indicates the lack of contribution by the SOFC in providing the reactive power of MG. In this MG, the battery is responsible for providing the MG with reactive power after the

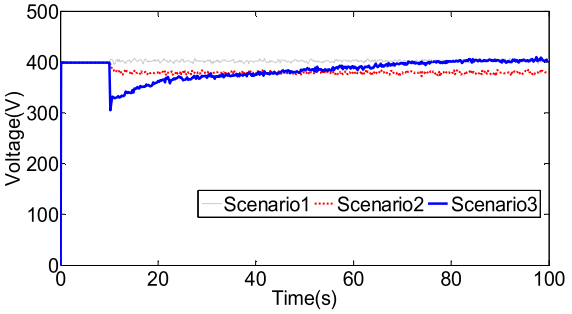

Fig. 15. Magnitude of Bus 11 voltage in various scenarios.

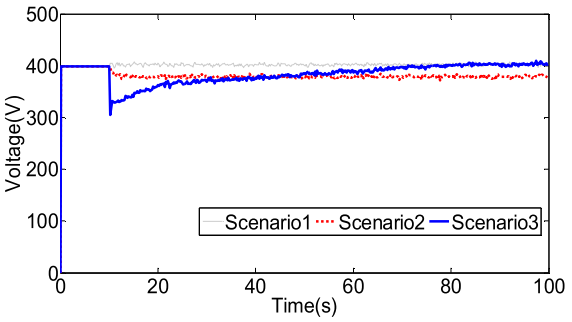

Fig. 16. Magnitude of Bus 10 voltage in various scenarios.

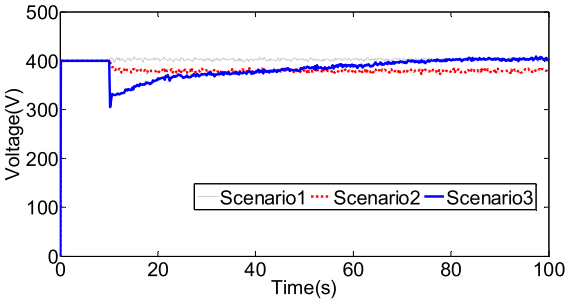

Fig. 17. Magnitude of Bus 9 voltage in various scenarios.

disconnection. SOFC plays its role in the secondary frequency control system and this system is the same in all three scenarios. For this reason, the results of three scenario are close to each other in Figs. 18 and 19. The proposed controller of this article has been added to the primary frequency control system to improve its performance. Fig. 20 shows the active power of PV system in various scenarios. It is observed that this power is similar in all scenarios prior to and after the disconnection and almost equal to 10 kW—the maximum value of the produced active power—due to the use of the MPPT system for taking maximum advantage of solar radiation. Fig. 21 depicts the reactive power output of PV system in different scenarios. This power is also

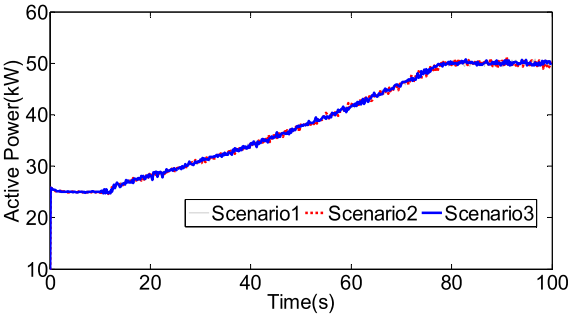

Fig. 18. SOFC active power in various scenarios.

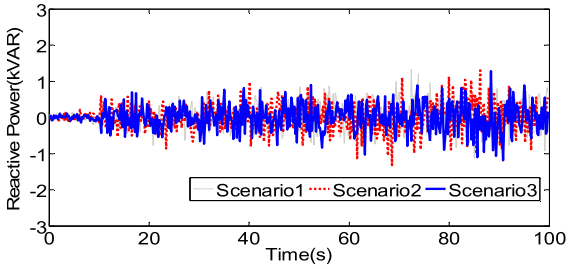

Fig. 19. SOFC reactive power in various scenarios.

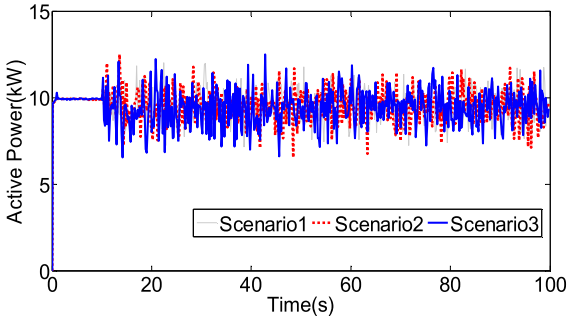

Fig. 20. PV active power in various scenarios.

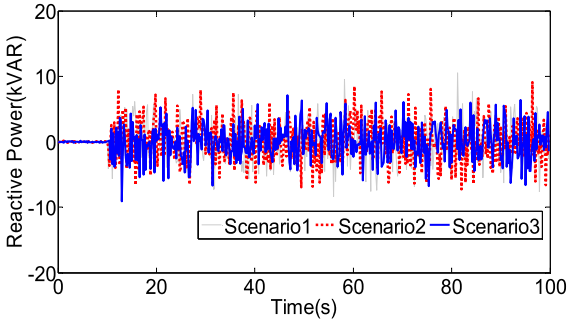

Fig. 21. PV reactive power in various scenarios.

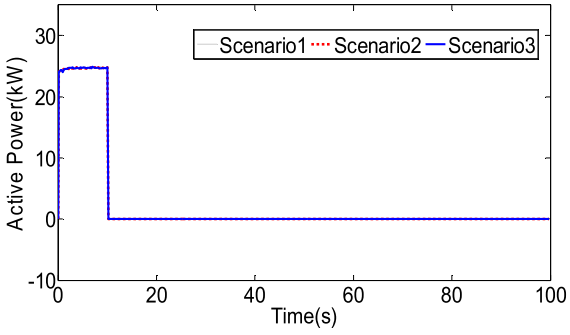

Fig. 22. Active power injected from the upstream grid.

similar for the various scenarios before and after the disconnection and equals to zero, which indicates the lack of participation by the PV in providing the microgrid with reactive power. PVs usually operate in the unity power factor mode and are not capable of generating reactive power. Figs. 22 and 23, respectively, sketch the active and reactive powers injected from the upstream grid to the microgrid in various scenarios. It can be observed in these figures that the grid performance is similar in all three scenarios. Before the disconnection, 25 kW of active power and 25 kVar of reactive power are injected from the upstream grid to the microgrid. However, after the disconnection, this power reduces to zero.

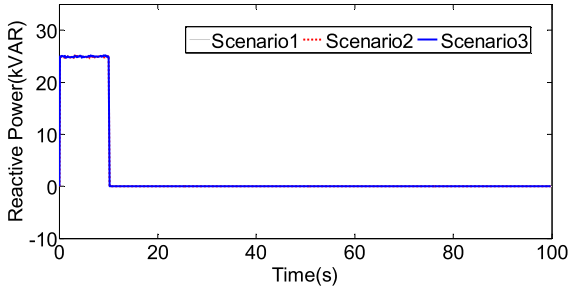

Fig. 23. Reactive power injected from the upstream grid.

5. Conclusion

In this paper, the idea of using frequency-reactive power channel to improve the performance of the frequency control system in an islanded microgrid was introduced. To implement this channel, a novel frequency-reactive power controller was proposed for controlling the inverter-interfaced energy storage devices (such as batteries) to the microgrid and added to the conventional frequency control system. The proposed controller causes the microgrid frequency to experience a smaller drop during contingencies and reduces the required battery capacity used to control the frequency. At the same time, the customer voltage would remain within permissible limits and comply with established standards. Moreover, a new factor denoted the frequency-reactive power factor (FRF) was introduced for each bus, and the mathematical relationships necessary for its computation were derived. This factor is used to determine the appropriate buses for installing the proposed frequency control system. As the obtained results show, the proposed control approach is more efficient compared to the conventional frequency control methods for microgrids.

This paper proposes a complementary technique to improve the performance of the conventional droop control techniques in transient conditions with the help of the voltage. You can even add this proposed technique to the transiently coupled droop control techniques and improve their transient performance in the frequency control. In this case, if we want to make a comparison we have to compare “the improved droop control methods without the proposed controller” with “the improved droop control methods with the proposed controller”. This can be done as a future work. The purpose of this paper is to present a new idea and prove its efficiency in improving the transient performance of a frequency control system. To this end, in this paper the proposed controller has been added to the conventional droop control techniques and, “the conventional droop control techniques without the proposed controller” have been compared with “the conventional droop control techniques with the proposed controller”. The results show a significant improvement in the performance of the conventional droop control techniques with the presence of the proposed controller. In conclusion, no comparison is needed between the results of this paper and the results of the transiently coupled droop control techniques. The proposed controller can also be implemented in multi-microgrid systems as future work. In addition, the potential of other reactive power sources such as capacitive banks, SVC and tap changers can be used for this purpose. Coordinated control of these equipments and the inverters is another issue to be analysed in future.

CRediT authorship contribution statement

Saeed Aminzadeh: Conceptualization, Software, Validation, Writing - original draft. **Mehrdad Tarafdar Hagh:** Conceptualization, Methodology, Validation, Writing - review & editing, Supervision. **Heresh Seyedi:** Conceptualization, Methodology, Validation, Writing - review & editing, Supervision.

Declaration of Competing Interest

The authors declare that they have no known competing financial interests or personal relationships that could have appeared to influence the work reported in this paper.

References

[1] Lopes PJA, Moreira CL, Madureira AG. Defining control strategies for microgrids islanded operation. IEEE Trans Power Syst 2006;21(2):916–24.
[2] Brabandere KD, Bolsens B, Keybus JVD. A voltage and frequency droop control method for parallel inverters. IEEE Trans Power Electron 2007;22(4):1107–15.
[3] Wu T, Liu Z, Liu J, et al. A unified virtual power decoupling method for droop-controlled parallel inverters in microgrids. IEEE Trans Power Electron 2016;31(8):5587–603.
[4] Huang X, Wang Z, Jiang J. Control and load-dispatching strategies for a *microgrid* with a DC/AC inverter of fixed *frequency*. Int J Electr Power Energy Syst 2012;43:1127–36.
[5] Wu X, Shen C, Iravani R. A distributed, cooperative frequency and voltage control for microgrids. IEEE Trans Smart Grid 2018:9(4).
[6] Sai Sesha VP, Kesanakurthy SS. Model predictive control approach for frequency and voltage control of standalone micro-grid. IET Gener Transm Distrib 2018;12(14):3405–13.
[7] John T, Lam SP. Voltage and frequency control during microgrid islanding in a multi-area multi-microgrid system. 2017; 11(6).
[8] Khederzadeh M, Maleki H, Asgharian V. *Frequency control* improvement of two adjacent *microgrids* in autonomous mode using back to back voltage-sourced converters. Int J Electr Power Energy Syst 2016;74(1):126–33.
[9] Zhao Z, Yang P, Guerrero JM, Xu Z, Green TC. 'Multiple-time-scales hierarchical frequency stability control strategy of medium-voltage isolated microgrid. IEEE Trans Power Electron 2016;31(8):5974–91.
[10] Chuang SJ, Hong CM, Chen CH. Design of intelligent *control* for stabilization of *microgrid* system. Int J Electr Power Energy Syst 2016;82(10):569–78.
[11] Sekhar PC, Mishra S. Storage free smart energy management for frequency control in a diesel-PV-fuel cell-based hybrid AC microgrid. IEEE Trans Neural Networks Learn Syst 2016;27(8):1657–71.
[12] Serban I, Marinescu C. Battery energy storage system for *frequency* support in *microgrids* and with enhanced *control* features for uninterruptible supply of local loads. Int J Electr Power Energy Syst 2014;54(1):431–41.
[13] Majumder R, Ledwich G, Ghosh A, et al. Droop control of converter-interfaced microsources in rural distributed generation. IEEE Trans Power Deliv 2010;25(4):2768–78.
[14] Khan H, Dasouki S, Sreeram V, et al. Universal active and reactive power control of electronically interfaced distributed generation sources in virtual power plants operating in grid-connected and islanding modes. IET Gener Transm Distrib 2013;7(8):885–97.
[15] Sun X, Tian Y, Chen Z. Adaptive decoupled power control method for inverter connected DG. IET Renew Power Gener 2013;8(2):171–82.
[16] Tang X, Hu X, Li N, et al. A novel frequency and voltage control method for islanded microgrid based on multienergy storages. IEEE Trans Smart Grid 2016;7(1):410–9.
[17] Kallamadi M, Sarkar V. Enhanced real-time power balancing of an AC microgrid through transiently coupled droop control. IET Gener Transm Distrib 2017;11(8):1933–42.
[18] Moslemi R, Mohammadpour J. Accurate reactive power control of autonomous microgrids using an adaptive virtual inductance loop. Electr Power Syst Res 2015;129:142–9.
[19] He J, Li YW. Analysis, design, and implementation of virtual impedance for power electronics interfaced distributed generation. IEEE Trans Ind Appl 2011;47(6):2525–38.
[20] Guerrero JM, Vicuña LG, Matas J, Castilla M, Miret J. Output impedance design of parallel-connected ups inverters with wireless load-sharing control. IEEE Trans Ind Appl 2005;52(4):1126–35.
[21] He J, Li YW, Guerrero JM, Blaabjerg F, Vasquez JC. An islanding microgrid power sharing approach using enhanced virtual impedance control scheme. IEEE Trans Power Electron 2013;28(11):5272–82.
[22] Mahmood H, Michaelson D, Jiang J. Accurate reactive power sharing in an islanded microgrid using adaptive virtual impedance. IEEE Trans Power Electron 2015;30(3):1605–17.
[23] Li Y, Li YW. Power management of inverter interfaced autonomous microgrid based on virtual frequency-voltage frame. IEEE Trans Smart Grid 2011;2(1):30–40.
[24] Kundur P. Power System Stability and Control. New York: McGraw- Hill; 1994.
[25] Saadat H. Power System Analysis. New Delhi: Tata McGraw-Hill; 2002.
[26] Arrillaga J, Watson NR, Che S. Power system quality assessment. John Wiley & Sons; 2000.